


Cite this: *RSC Adv.*, 2019, 9, 41913

Received 12th November 2019

Accepted 11th December 2019

DOI: 10.1039/c9ra09421k

rsc.li/rsc-advances

Selective loading of platinum or silver cocatalyst onto a hydrogen-evolution photocatalyst in a silver-mediated all solid-state Z-scheme system for enhanced overall water splitting†

Junya Osaki,^a Masaomi Yoda,^a Toshihiro Takashima^{id}^{ab} and Hiroshi Irie^{id}^{*ab}

We selectively loaded a hydrogen (H₂)-evolution cocatalyst, either platinum (Pt) or silver (Ag), onto a H₂-evolution photocatalyst, zinc rhodium oxide (ZnRh₂O₄), in a Ag-inserted ZnRh₂O₄ and bismuth vanadium oxide (Bi₄V₂O₁₁) hetero-junction photocatalyst (ZnRh₂O₄/Ag/Bi₄V₂O₁₁) by a photo-deposition method. The selective loading of Pt or Ag was achieved by taking advantage of the band-gap difference between ZnRh₂O₄ (1.2 eV) and Bi₄V₂O₁₁ (1.7 eV) and increased the overall water-splitting activity of the photocatalyst.

Hydrogen (H₂) is a versatile, non-polluting energy carrier because the chemical energy stored in the H–H bond is released when H₂ combines with oxygen (O₂) and yields only water as the reaction product. Accordingly, an energy infrastructure based on H₂ represents an ideal solution to energy-related environmental issues for reducing carbon dioxide (CO₂) emissions. Photocatalytic water-splitting using sunlight represents one of the cleanest methods to produce H₂.¹ Since the Honda–Fujishima effect was first reported in 1972,² various water-splitting methods, including electrode and powder systems, have been extensively investigated for the possibility of simple, large scale production of H₂.^{2,3} Following the demonstration by Domen and coworkers that a solid solution of gallium nitride (GaN)–zinc oxide (ZnO) is capable of splitting water at wavelengths up to ~480 nm,⁴ numerous researchers have attempted to identify powdered photocatalysts that utilize longer wavelengths of visible light for efficient water-splitting using solar energy.⁵

Previously, we fabricated a hetero-junction photocatalyst consisting of zinc rhodium oxide (ZnRh₂O₄) and bismuth vanadium oxide (Bi₄V₂O₁₁), which functioned as H₂- and O₂-evolution photocatalysts, respectively, and either silver (Ag) or gold (Au) as a conductive layer (ZnRh₂O₄/Ag/Bi₄V₂O₁₁ or ZnRh₂O₄/Au/Bi₄V₂O₁₁) after Tada and coworkers.⁶ Recently, similar hetero-junction photocatalysts were reported.⁷

In ZnRh₂O₄/Ag/Bi₄V₂O₁₁ or ZnRh₂O₄/Au/Bi₄V₂O₁₁, overall pure water-splitting proceeded under irradiation with red light

(wavelengths larger than 700 nm)^{8–10} via Ag or Au, which mediated the transfer of photo-excited electrons from the conduction band (CB) of Bi₄V₂O₁₁ to the valence band (VB) of ZnRh₂O₄. Thus, the photo-excited electrons in ZnRh₂O₄ and holes in Bi₄V₂O₁₁ effectively reduced and oxidized water, respectively, to accomplish overall water splitting. The modification of the cocatalyst with a metal or metal oxide is essential to enhance the water-splitting activity. The selective loading of a H₂-favorable cocatalyst onto ZnRh₂O₄ is expected to increase H₂ evolution and thereby increase the overall water-splitting activity of this hetero-junction photocatalyst. Here, we used platinum (Pt) and Ag as H₂-evolution cocatalysts and attempted to selectively deposit Pt or Ag onto ZnRh₂O₄ in ZnRh₂O₄/Ag/Bi₄V₂O₁₁.

Powdered ZnRh₂O₄/Ag/Bi₄V₂O₁₁ (molar ratio of ZnRh₂O₄ to Bi₄V₂O₁₁ was 1.0 : 1.2) was prepared following procedures previously reported procedures (ESI-1†)⁸ and the photo-deposition of Pt or Ag was conducted under light irradiation at wavelength longer than 850 nm. Under these irradiation conditions, only ZnRh₂O₄ was photo-excited because the energy of irradiated light was higher than band-gap energy of ZnRh₂O₄ (1.2 eV) but smaller than that of Bi₄V₂O₁₁ (1.7 eV). Due to the specific photoexcitation of ZnRh₂O₄, Pt or Ag was only photo-deposited onto this material, generating Pt/ZnRh₂O₄/Ag/Bi₄V₂O₁₁ and Ag/ZnRh₂O₄/Ag/Bi₄V₂O₁₁ (ESI-1†).

In the powder XRD pattern of ZnRh₂O₄/Ag/Bi₄V₂O₁₁ (Fig. S1, ESI-2†), the observed peaks mainly corresponded to two phases originating from ZnRh₂O₄ and Bi₄V₂O₁₁, with the trace peaks ascribed to an unknown Ag oxide (likely AgVO₃). Notably, no Ag peaks were observed in the XRD spectrum, which is plausible since the amount of Ag remaining in the composite was too small for detection. These observations are consistent with those reported previously.⁸ The valency of Ag in the

^aSpecial Doctoral Program for Green Energy Conversion Science and Technology, Integrated Graduate School of Medicine, Engineering, and Agricultural Sciences, University of Yamanashi, 4-3-11 Takeda, Kofu, Yamanashi 400-8511, Japan

^bClean Energy Research Center, University of Yamanashi, 4-3-11 Takeda, Kofu, Yamanashi 400-8511, Japan. E-mail: hirie@yamanashi.ac.jp

† Electronic supplementary information (ESI) available. See DOI: 10.1039/c9ra09421k



photocatalyst was determined by XPS to be mainly zero (Ag^0). The implications of this finding are discussed below.

UV-vis absorption spectra of $\text{ZnRh}_2\text{O}_4/\text{Ag}/\text{Bi}_4\text{V}_2\text{O}_{11}$, $\text{Pt}/\text{ZnRh}_2\text{O}_4/\text{Ag}/\text{Bi}_4\text{V}_2\text{O}_{11}$, and $\text{Ag}/\text{ZnRh}_2\text{O}_4/\text{Ag}/\text{Bi}_4\text{V}_2\text{O}_{11}$ are shown in Fig. 1. In the spectra, $\text{Pt}/\text{ZnRh}_2\text{O}_4/\text{Ag}/\text{Bi}_4\text{V}_2\text{O}_{11}$ and $\text{Ag}/\text{ZnRh}_2\text{O}_4/\text{Ag}/\text{Bi}_4\text{V}_2\text{O}_{11}$ had greater absorption than that of $\text{ZnRh}_2\text{O}_4/\text{Ag}/\text{Bi}_4\text{V}_2\text{O}_{11}$ in the longer wavelength region, a property that is derived from the deposited Pt and Ag.

Fig. 2a–f show XPS spectra of $\text{ZnRh}_2\text{O}_4/\text{Ag}/\text{Bi}_4\text{V}_2\text{O}_{11}$, $\text{Pt}/\text{ZnRh}_2\text{O}_4/\text{Ag}/\text{Bi}_4\text{V}_2\text{O}_{11}$, and $\text{Ag}/\text{ZnRh}_2\text{O}_4/\text{Ag}/\text{Bi}_4\text{V}_2\text{O}_{11}$ for Bi 4f (Fig. 2a), V 2p (Fig. 2b), Zn 2p (Fig. 2c), Rh 3d (Fig. 2d), Ag 3d (Fig. 2e), and Pt 4f (Fig. 2f). As we assumed that the cocatalyst, Pt or Ag, was selectively deposited onto ZnRh_2O_4 and the $\text{Bi}_4\text{V}_2\text{O}_{11}$ surface remained unaltered after the deposition of the cocatalyst, all of the XPS peaks were normalized using the peak areas of Bi 4f for the bare, Pt-deposited, and Ag-deposited $\text{ZnRh}_2\text{O}_4/\text{Ag}/\text{Bi}_4\text{V}_2\text{O}_{11}$ photocatalysts (Fig. 2a). It was reasonable that the peak areas in the normalized V 2p_{3/2} spectra of the three photocatalysts were similar (Fig. 2b). Further, the normalized Zn 2p and Rh 3d peaks of $\text{Pt}/\text{ZnRh}_2\text{O}_4/\text{Ag}/\text{Bi}_4\text{V}_2\text{O}_{11}$ and $\text{Ag}/\text{ZnRh}_2\text{O}_4/\text{Ag}/\text{Bi}_4\text{V}_2\text{O}_{11}$ were smaller than those of $\text{ZnRh}_2\text{O}_4/\text{Ag}/\text{Bi}_4\text{V}_2\text{O}_{11}$ (Fig. 2c and d). The results of the surface-sensitive XPS measurements indicate that Pt and Ag were selectively deposited onto ZnRh_2O_4 .

The normalized Ag 3d peak area of $\text{Pt}/\text{ZnRh}_2\text{O}_4/\text{Ag}/\text{Bi}_4\text{V}_2\text{O}_{11}$ was quite similar to that of $\text{ZnRh}_2\text{O}_4/\text{Ag}/\text{Bi}_4\text{V}_2\text{O}_{11}$ (Fig. 2e). This result is reasonable because the Ag 3d spectra of the two photocatalysts are attributable to the Ag inserted between ZnRh_2O_4 and $\text{Bi}_4\text{V}_2\text{O}_{11}$. In contrast, the Ag 3d spectrum of $\text{Ag}/\text{ZnRh}_2\text{O}_4/\text{Ag}/\text{Bi}_4\text{V}_2\text{O}_{11}$ was larger than those of $\text{Pt}/\text{ZnRh}_2\text{O}_4/\text{Ag}/\text{Bi}_4\text{V}_2\text{O}_{11}$ and $\text{ZnRh}_2\text{O}_4/\text{Ag}/\text{Bi}_4\text{V}_2\text{O}_{11}$, indicating that the former spectrum originated from the photo-deposited Ag and Ag located between ZnRh_2O_4 and $\text{Bi}_4\text{V}_2\text{O}_{11}$. In the normalized Pt 4f spectra, the Pt 4f peaks were only observed on $\text{Pt}/\text{ZnRh}_2\text{O}_4/\text{Ag}/\text{Bi}_4\text{V}_2\text{O}_{11}$ and were not detected in the XPS spectra of $\text{Ag}/\text{ZnRh}_2\text{O}_4/\text{Ag}/\text{Bi}_4\text{V}_2\text{O}_{11}$ and $\text{ZnRh}_2\text{O}_4/\text{Ag}/\text{Bi}_4\text{V}_2\text{O}_{11}$ (Fig. 2f).

To quantitatively analyze the amounts and determine the valencies of Pt and Ag in the three photocatalysts, a peak deconvolution method was applied to the Bi 4f, Ag 3d, and Pt 4f spectra (Fig. S2 in ESI-3[†]). As we considered that the $\text{Bi}_4\text{V}_2\text{O}_{11}$ surface remained unaltered after the Pt or Ag deposition, we

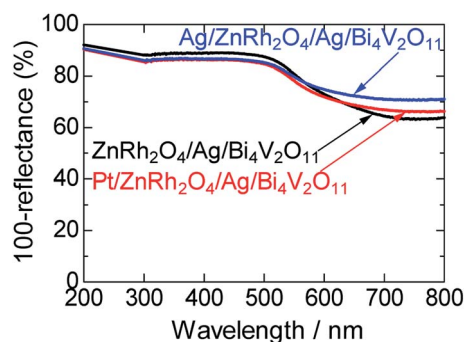


Fig. 1 UV-visible absorption spectra of $\text{ZnRh}_2\text{O}_4/\text{Ag}/\text{Bi}_4\text{V}_2\text{O}_{11}$, $\text{Pt}/\text{ZnRh}_2\text{O}_4/\text{Ag}/\text{Bi}_4\text{V}_2\text{O}_{11}$, and $\text{Ag}/\text{ZnRh}_2\text{O}_4/\text{Ag}/\text{Bi}_4\text{V}_2\text{O}_{11}$.

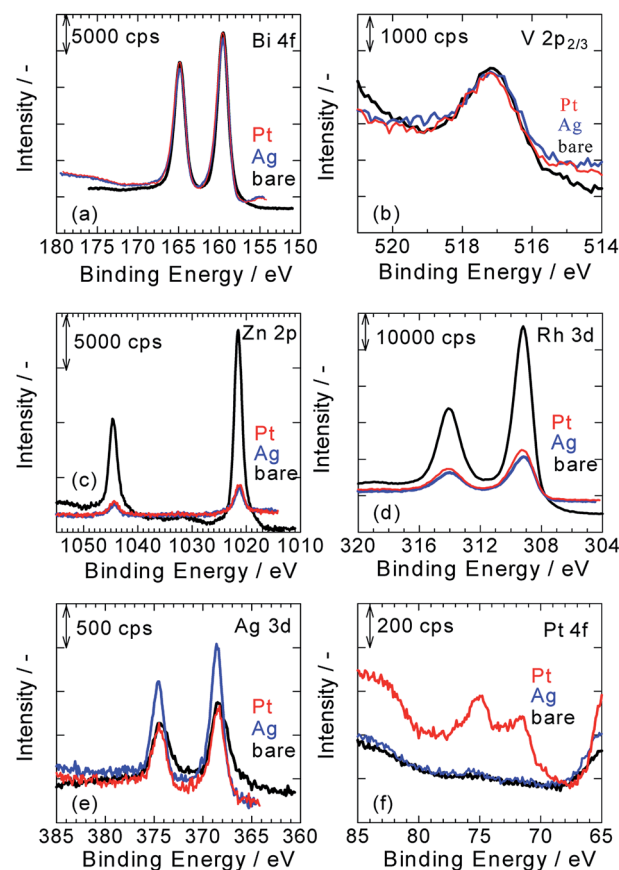


Fig. 2 Normalized XPS spectra of $\text{ZnRh}_2\text{O}_4/\text{Ag}/\text{Bi}_4\text{V}_2\text{O}_{11}$ (black lines), $\text{Pt}/\text{ZnRh}_2\text{O}_4/\text{Ag}/\text{Bi}_4\text{V}_2\text{O}_{11}$ (red lines), and $\text{Ag}/\text{ZnRh}_2\text{O}_4/\text{Ag}/\text{Bi}_4\text{V}_2\text{O}_{11}$ (blue lines) for Bi 4f (a), V 2p (b), Zn 2p (c), Rh 3d (d), Ag 3d (e), and Pt 4f (f). All spectra were calibrated with the C 1s peak, which was derived from a surface-contaminant hydrocarbon with a binding energy of 284.5 eV.

estimated the amount of Pt or Ag in the photocatalysts based on the amount of Bi. First, peak deconvolution for Bi 4f was performed with the following parameters. The binding energies of $\text{Bi } 4f_{7/2}$ and $\text{Bi } 4f_{5/2}$ of Bi^{3+} were fixed at 159.5 ± 0.1 eV and 164.8 ± 0.1 eV, respectively.¹¹ For the Pt- and Ag-deposited photocatalysts, an additional pair of small peaks was observed at 161.0 ± 0.1 eV and 166.3 ± 0.1 eV. The origin of the additional peaks was unclear; however, the peaks were likely derived from $\text{Bi}^{3+}\text{-Cl}^-$ (e.g., BiOCl)¹² or $\text{Bi}^{3+}\text{-NO}_3^-$ ($\text{Bi}(\text{NO}_3)_3$) remaining on the surface because Pt or Ag was photo-deposited in the $\text{H}_2\text{-PtCl}_6 \cdot 6\text{H}_2\text{O}$ or AgNO_3 solution despite thorough washing with distilled water. The peak area ratio of $\text{Bi } 4f_{5/2}$ to $\text{Bi } 4f_{7/2}$ for Bi^{3+} was fixed at 0.75 (Fig. S2a, S2c, S2f and Table S1 in ESI-3[†]).

In Fig. S2b, S2d, and S2g in ESI-3,† the Ag 3d peaks for the three photocatalysts were deconvoluted by a pair of Ag 3d peaks ($\text{Ag } 3d_{5/2}$ and $\text{Ag } 3d_{3/2}$, with binding energies of 368.6 ± 0.1 eV and 374.6 ± 0.1 eV, respectively), which is attributable to metallic Ag (Ag^0).^{8,9,13} These results indicate that Ag was inserted as a metallic particle between ZnRh_2O_4 and $\text{Bi}_4\text{V}_2\text{O}_{11}$ in $\text{ZnRh}_2\text{O}_4/\text{Ag}/\text{Bi}_4\text{V}_2\text{O}_{11}$, $\text{Pt}/\text{ZnRh}_2\text{O}_4/\text{Ag}/\text{Bi}_4\text{V}_2\text{O}_{11}$, and $\text{Ag}/\text{ZnRh}_2\text{O}_4/\text{Ag}/\text{Bi}_4\text{V}_2\text{O}_{11}$.^{8,9} In addition, the Ag cocatalyst was also proved to be deposited as the metallic one. In contrast, the Pt 4f



peaks for Pt/ZnRh₂O₄/Ag/Bi₄V₂O₁₁ were deconvoluted by three pairs of Pt 4f peaks with binding energies of 71.3 eV (Pt 4f_{7/2}) and 74.6 eV (Pt 4f_{5/2}) for metallic Pt (Pt⁰), 72.3 eV (Pt 4f_{7/2}) and 75.6 eV (Pt 4f_{5/2}) for Pt²⁺, and 73.3 eV (Pt 4f_{7/2}) and 76.6 eV (Pt 4f_{5/2}) for Pt³⁺ (Fig. S2e in ESI-3†).¹⁴ The total Pt⁰, Pt²⁺, and Pt³⁺ areas were determined by summing the corresponding deconvolution areas of Pt 4f_{5/2} and Pt 4f_{7/2} (Table S1 in ESI-3†). The atomic ratios of Pt⁰, Pt²⁺, and Pt³⁺ vs. total Pt were calculated to be 0.63, 0.25, and 0.12, respectively, and by dividing the total Pt⁰, Pt²⁺, and Pt³⁺ areas by the total Pt area and represent the sum of the total Pt⁰, Pt²⁺, and Pt³⁺ areas. Thus, the major Pt species that functioned as the cocatalyst was Pt⁰; however, Pt⁴⁺ was not fully reduced to Pt⁰. The valence distribution was not observed for Ag, but observed for Pt. We are considering two possible explanations; one is a difference in the reduction potential between Ag and Pt deposition, Ag⁺ + e⁻ → Ag⁰ (0.80 V vs. SHE), PtCl₆²⁻ + 2e⁻ → PtCl₄²⁻ + 2Cl⁻ (Pt⁴⁺ → Pt²⁺, 0.68 V vs. SHE), PtCl₄²⁻ + 2e⁻ → Pt⁰ + 4Cl⁻ (Pt²⁺ → Pt⁰, 0.72 V vs. SHE) although that of PtCl₆²⁻ + e⁻ → PtCl₅²⁻ + Cl⁻ is unknown. Thus, forming Ag⁰ from the reduction of Ag⁺ is thermodynamically more favorable than forming Pt²⁺ from that of Pt⁴⁺ and Pt⁰ from that of Pt²⁺. The other reason is that the reduction product from Ag⁺ is only Ag⁰, but some reduction products are possible from Pt⁴⁺, such as Pt³⁺, Pt²⁺, Pt⁺, and Pt⁰, if the reduction proceeds. In fact, Pt⁴⁺ was not detected, and the reduction of Pt⁴⁺ proceeded.

The Ag and Bi areas were determined by summing the deconvolution areas of Ag 3d_{5/2} and Ag 3d_{3/2}, and those of Bi 4f_{7/2} and Bi 4f_{5/2}, respectively (Table S1 in ESI-3†). The atomic ratio of Ag to Bi was then calculated based on the Ag 3d (5.99) and Bi 4f sensitivity factors (9.14),¹⁵ and the mole percent of Ag to that of the sum of ZnRh₂O₄ and Bi₄V₂O₁₁ (1.0 mole of ZnRh₂O₄ + 1.2 mole of Bi₄V₂O₁₁) was determined. The weight percent (wt%) of Ag in the three photocatalysts was recalculated (Table S2 in ESI-3†). As expected, the amount of Ag in ZnRh₂O₄/Ag/Bi₄V₂O₁₁ and Pt/ZnRh₂O₄/Ag/Bi₄V₂O₁₁ was identical at 2.1 wt%. Thus, the Ag cocatalyst deposited in Ag/ZnRh₂O₄/Ag/Bi₄V₂O₁₁ was estimated to be 1.1 wt% based on the assumption that the amount of Ag inserted in Ag/ZnRh₂O₄/Ag/Bi₄V₂O₁₁ was 2.1 wt%. Similarly, the amount of Pt cocatalyst in Pt/ZnRh₂O₄/Ag/Bi₄V₂O₁₁ was calculated to be 1.2 wt% (Table S2† in ESI-3†) based on the total Pt area and Pt 4f sensitivity factor (5.575).¹⁵

SEM images of ZnRh₂O₄/Ag/Bi₄V₂O₁₁, Pt/ZnRh₂O₄/Ag/Bi₄V₂O₁₁, and Ag/ZnRh₂O₄/Ag/Bi₄V₂O₁₁ powders are shown (Figs. S3a–c in ESI-4†). All images were quite similar, and small ZnRh₂O₄ (~200 nm) and large Bi₄V₂O₁₁ (~10 μm) particles can be clearly observed. However, the photo-deposited Pt and Ag were not observed.

STEM imaging (high angle annular dark-field (HAADF), bright-field (BF)) and EDS-based elemental mapping of Pt/ZnRh₂O₄/Ag/Bi₄V₂O₁₁ were performed (Fig. 3a–g). In the HAADF-STEM image (Fig. 3a), ZnRh₂O₄ and Bi₄V₂O₁₁ particles were clearly distinguishable based on the SEM image (Fig. S3b in ESI-4†) and their previously reported sizes of ~200 nm and ~10 μm, respectively.⁸ Thus, the small aggregated particles in the HAADF-STEM image were ZnRh₂O₄ and were adjacent to a large particle of Bi₄V₂O₁₁. The particle compositions were

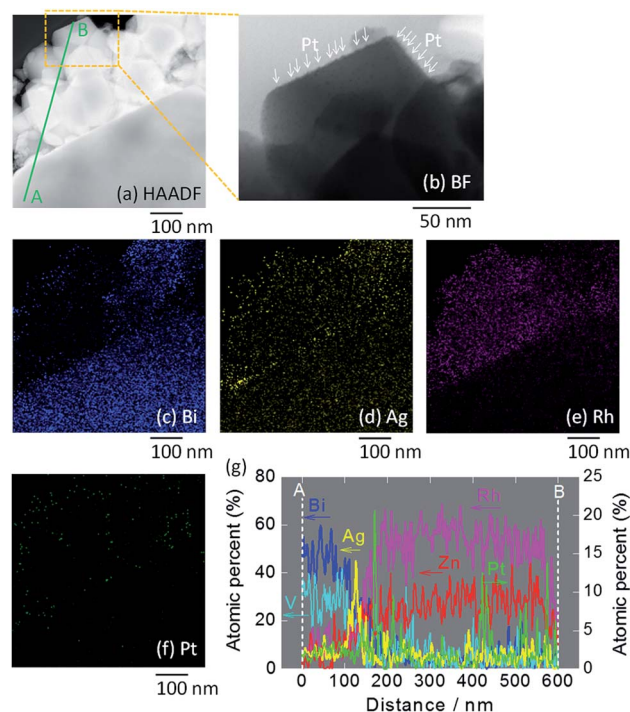


Fig. 3 STEM images of Pt/ZnRh₂O₄/Ag/Bi₄V₂O₁₁. HAADF-STEM image (a) and the BF enlargement (b) in which Pt is indicated by arrows, and EDS elemental maps (c–f), in which blue (c), yellow (d), pink (e), and green (f) colors correspond to Bi, Ag, Rh, and Pt, respectively. In (a), the line along which the elemental analysis was performed is shown (A to B). Atomic percentages of Bi, V, Zn, Rh, Ag, and Pt measured from the area of Bi₄V₂O₁₁ (A) to that of ZnRh₂O₄ (B) (g). Enlarged images of (a)–(f) are shown in ESI-5.†

confirmed by the EDS-based elemental mapping of Bi and Rh in Fig. 3c and e, respectively. In addition, Ag particles were detected (Fig. 3d) between the areas of Bi (Fig. 3c) and Rh (Fig. 3e), indicating that Ag was inserted between the ZnRh₂O₄ and Bi₄V₂O₁₁ particles. This finding was also confirmed by the line elemental analysis (Fig. 3g). Notably, the atomic percentages of Bi and V decreased at the boundary of Ag and ZnRh₂O₄, and those of Zn and Rh increased at the boundary of Ag and Bi₄V₂O₁₁. Accordingly, the percentage of Ag increased and

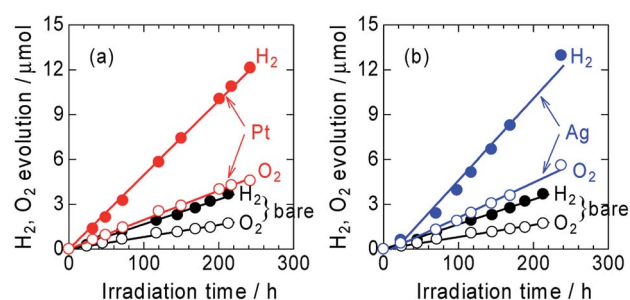


Fig. 4 Time courses of photocatalytic evolution of H₂ and O₂ from water over Pt/ZnRh₂O₄/Ag/Bi₄V₂O₁₁ (a) and Ag/ZnRh₂O₄/Ag/Bi₄V₂O₁₁ (b) irradiated with 700 nm LED light. For comparison, the evolution of H₂ and O₂ over bare ZnRh₂O₄/Ag/Bi₄V₂O₁₁ is also shown.



Table 1 Light intensity, H₂ generation rates, and AQE values in the presence of ZnRh₂O₄/Ag/Bi₄V₂O₁₁, Pt/ZnRh₂O₄/Ag/Bi₄V₂O₁₁ and Ag/ZnRh₂O₄/Ag/Bi₄V₂O₁₁

Light source	Light/mW cm ⁻²	H ₂ evolution rate/μmol h ⁻¹	AQE/%
ZnRh ₂ O ₄ /Ag/Bi ₄ V ₂ O ₁₁	2.9	1.7×10^{-2}	1.5×10^{-2}
Pt/ZnRh ₂ O ₄ /Ag/Bi ₄ V ₂ O ₁₁	3.5	5.0×10^{-2}	4.1×10^{-2}
Ag/ZnRh ₂ O ₄ /Ag/Bi ₄ V ₂ O ₁₁	3.5	5.5×10^{-2}	4.6×10^{-2}

decreased at the boundary with Bi₄V₂O₁₁ and ZnRh₂O₄, respectively, indicating that Ag was present at the Bi₄V₂O₁₁ and ZnRh₂O₄ interface. As expected, Pt was only deposited onto ZnRh₂O₄ because Pt was only distributed in the vicinity of Rh (Fig. 3f). This finding was also confirmed by the line elemental analysis, as several sharp peaks derived from Pt were observed in the area of ZnRh₂O₄ (Fig. 3g). In addition, extremely small particles, corresponding to Pt, were observed only on ZnRh₂O₄ in the enlarged BF image of Pt/ZnRh₂O₄/Ag/Bi₄V₂O₁₁ (Fig. 3b).

The time courses of H₂ and O₂ evolution from Pt/ZnRh₂O₄/Ag/Bi₄V₂O₁₁ and Ag/ZnRh₂O₄/Ag/Bi₄V₂O₁₁ in comparison with ZnRh₂O₄/Ag/Bi₄V₂O₁₁ under monochromic light irradiation at a wavelength of 700 nm were measured (Fig. 4a and b). The three photocatalysts evolved H₂ and O₂ from water at a molar ratio of ~2 to 1 (2.1 to 1, 2.3 to 1, and 2.2 to 1 for ZnRh₂O₄/Ag/Bi₄V₂O₁₁, Pt/ZnRh₂O₄/Ag/Bi₄V₂O₁₁, and Ag/ZnRh₂O₄/Ag/Bi₄V₂O₁₁, respectively), indicating that the overall water-splitting reaction proceeded efficiently. The band alignments of ZnRh₂O₄, Ag, and Bi₄V₂O₁₁, and the charge transfer process are shown in Scheme S1 (ESI-6†). The photo-excited electrons in ZnRh₂O₄ and holes in Bi₄V₂O₁₁ can effectively reduce and oxidize water, respectively. Specifically, Ag acted as a solid-state electron mediator for the electron transfer from the CB of Bi₄V₂O₁₁ to the VB of ZnRh₂O₄. The deposition of Pt or Ag enhanced the H₂ and O₂ evolution rates, demonstrating that Pt and Ag functioned as cocatalysts for the overall water-splitting reaction. The apparent quantum efficiency (AQE) values for the reaction over Pt/ZnRh₂O₄/Ag/Bi₄V₂O₁₁ ($4.1 \times 10^{-2}\%$) and Ag/ZnRh₂O₄/Ag/Bi₄V₂O₁₁ ($4.6 \times 10^{-2}\%$) were ~3-fold higher than that over ZnRh₂O₄/Ag/Bi₄V₂O₁₁ ($1.5 \times 10^{-2}\%$) (Tables 1 and S3 in ESI-7†).

We previously reported that the treatment of ZnRh₂O₄/Ag/Bi₄V₂O₁₁ with nitric acid (HNO₃) is required to achieve overall water splitting (ESI-1†). The treatment removes excess Ag containing Ag⁺ which is a sacrificial agent for O₂ evolution.^{8,9} Thus, without HNO₃ treatment, excess Ag remaining on Bi₄V₂O₁₁ in ZnRh₂O₄/Ag/Bi₄V₂O₁₁ evolves O₂ even from water, resulting in more O₂ being released than that of the stoichiometric amount of O₂ to H₂ of ~1 to 2. However, in the present study, H₂ and O₂ were evolved at a 2 : 1 ratio, providing further evidence that Ag was selectively deposited onto ZnRh₂O₄. Notably, Ag-deposited ZnRh₂O₄ is unable to evolve O₂ from water because the VB top potential of ZnRh₂O₄ lies at ~0.1 V (vs. SHE, pH = 0),¹⁶ which is thermodynamically unfavorable for O₂ evolution.

In conclusion, Pt or Ag as a cocatalyst was selectively photo-deposited onto ZnRh₂O₄ in ZnRh₂O₄/Ag/Bi₄V₂O₁₁ and resulted in the enhancement of stoichiometric H₂ and O₂ evolution from

water. ZnRh₂O₄/Ag/Bi₄V₂O₁₁ also has the potential to reduce CO₂ under visible-light irradiation to carbon monoxide (CO), formate, methanol, methane, and other hydrocarbons using water as an electron source. Notably, when present on ZnRh₂O₄, Ag acts as a selective cocatalyst for the conversion of CO₂ to CO. In contrast, as Pt lacks this property, different reaction products can be detected. Such studies are currently underway in our laboratory.

Conflicts of interest

There are no conflicts to declare.

Acknowledgements

This work was supported by JSPS KAKENHI (Grant-in-Aid for Scientific Research) (B), Grant Number 17H03126. We express gratitude to Mr G. Newton for the careful reading of the manuscript.

Notes and references

- 1 R. M. Navarro, M. A. Pena and J. L. G. Fierro, *Chem. Rev.*, 2007, **107**, 3952–3991.
- 2 A. Fujishima and K. Honda, *Nature*, 1972, **238**, 37–38.
- 3 O. Khaselev and J. A. Turner, *Science*, 1998, **280**, 425–427; W. J. Youngblood, S.-H. A. Lee, Y. Kobayashi, E. A. Hernandez-Pagan, P. G. Hoertz, T. A. Moore, A. L. Moore, D. Gust and T. E. Mallouk, *J. Am. Chem. Soc.*, 2009, **131**, 926–927; S. Y. Reece, J. A. Hamel, K. Sung, T. D. Jarvi, A. J. Esswein, J. J. H. Pijpers and D. G. Nocera, *Science*, 2011, **334**, 645–648; M. R. Singh, K. Papadantonakis, C. Xiang and N. S. Lewis, *Energy Environ. Sci.*, 2015, **8**, 2760–2767; S. Haussener, C. Xiang, J. M. Spurgeon, S. Ardo, N. S. Lewis and A. Z. Weber, *Energy Environ. Sci.*, 2012, **5**, 9922–9935; M. R. Singh, C. Xiang and N. S. Lewis, *Sustainable Energy Fuels*, 2017, **1**, 458–466; M. G. Walter, E. L. Warren, J. R. McKone, S. W. Boettcher, Q. Mi, E. A. Santori and N. S. Lewis, *Chem. Rev.*, 2010, **110**, 6446–6473; T. R. Cook, D. K. Dogutan, S. Y. Reece, Y. Surendranath, T. S. Teets and D. G. Nocera, *Chem. Rev.*, 2010, **110**, 6474–6502; K. Maeda and K. Domen, *J. Phys. Chem. Lett.*, 2010, **1**, 2655–2661.
- 4 K. Maeda, K. Teramura, D. Lu, T. Takata, N. Saito, Y. Inoue and K. Domen, *Nature*, 2006, **440**, 295.
- 5 L. Liao, Q. Zhang, Z. Su, Z. Zhao, Y. Wang, Y. Li, X. Lu, D. Wei, G. Feng, Q. Yu, *et al.*, *Nat. Nanotechnol.*, 2014, **9**,



- 69–73; C. Pan, T. Takata, M. Nakabayashi, T. Matsumoto, N. Shibata, Y. Ikumura and K. Domen, *Angew. Chem., Int. Ed.*, 2015, **54**, 2955–2959; J. Liu, Y. Liu, N. Liu, Y. Han, X. Zhang, H. Huang, Y. Lifshitz, S. T. Lee, J. Zhong and Z. Kang, *Science*, 2015, **347**, 970–974.
- 6 H. Tada, T. Mitsui, T. Kiyonaga, T. Akita and K. Tanaka, *Nat. Mater.*, 2006, **5**, 782–786.
- 7 Y. Sasaki, H. Nemoto, K. Saito and A. Kudo, *J. Phys. Chem. C*, 2009, **113**, 17536–17542; A. Iwase, Y. H. Ng, Y. Ishiguro, A. Kudo and R. Amal, *J. Am. Chem. Soc.*, 2011, **133**, 11054–11057; Z. Pan, T. Hisatomi, Q. Wang, S. Chen, M. Nakabayashi, N. Shibata, C. Pan, T. Takata, M. Katayama, T. Minegishi, A. Kudo and K. Domen, *ACS Catal.*, 2016, **6**, 7188–7196; Q. Wang, T. Hisatomi, Q. Jia, H. Tokudome, M. Zhong, C. Wang, Z. Pan, T. Takata, M. Nakabayashi, N. Shibata, Y. Li, I. D. Sharp, A. Kudo, T. Yamada and K. Domen, *Nat. Mater.*, 2016, **15**, 611–615; S. Sun, T. Hisatomi, Q. Wang, S. Chen, G. Ma, J. Liu, S. Nandy, T. Minegishi, M. Katayama and K. Domen, *ACS Catal.*, 2018, **8**, 1690–1696.
- 8 R. Kobayashi, K. Kurihara, T. Takashima, B. Ohtani and H. Irie, *J. Mater. Chem. A*, 2016, **4**, 3061–3067.
- 9 R. Kobayashi, T. Takashima, S. Tanigawa, S. Takeuchi, B. Ohtani and H. Irie, *Phys. Chem. Chem. Phys.*, 2016, **18**, 27693–28378.
- 10 K. Kamijyo, T. Takashima, M. Yoda, J. Osaki and H. Irie, *Chem. Commun.*, 2018, **54**, 7999–8002.
- 11 Q. Jia, K. Iwashima and A. Kudo, *Proc. Natl. Acad. Sci. U. S. A.*, 2012, **109**, 11564–11569.
- 12 L. Ye, K. Deng, F. Xe, L. Tian, T. Peng and L. Zan, *Phys. Chem. Chem. Phys.*, 2012, **14**, 82–85.
- 13 G. B. Houflund, Z. F. Hazos and G. N. Salaita, *Phys. Rev. B: Condens. Matter Mater. Phys.*, 2000, **62**, 4482–4486; K. Kuribayashi and S. Kitamura, *Thin Solid Films*, 2001, **400**, 160–164.
- 14 Y. Abe, H. Yanagizawa and K. Sasaki, *Jpn. J. Appl. Phys.*, 1998, **37**, 11126–11133.
- 15 A. J. Bard, R. Parsons and J. Jordan, *Standard Potentials in Aqueous Solution*, 1985, New York, Marcel Dekker.
- 16 Y. Takimoto, T. Kitta and H. Irie, *Int. J. Hydrogen Energy*, 2012, **37**, 134–138.

